ARTICLE

ACS chemical biology

Rationally Designed Inhibitors Identify STAT3 N-Domain as a Promising Anticancer Drug Target

Olga A. Timofeeva[†,‡], Vadim Gaponenko[§], Stephen J. Lockett[¶], Sergey G. Tarasov[∥], Sheng Jiang[**], Christopher J. Michejda[,††], Alan O. Perantoni[†], and Nadya I. Tarasova[**,*]**

[†]Laboratory of Comparative Carcinogenesis, National Cancer Institute, NCI-Frederick, Maryland 21702, [‡]Department of Oncology, Lombardi Comprehensive Cancer Center, Georgetown University Medical Center, Washington, DC 20057, [§]Department of Biochemistry and Molecular Genetics, University of Illinois in Chicago, Chicago, Illinois 60607, [¶]Image Analysis Laboratory, SAIC-Frederick, Inc., Frederick, Maryland 21702, [∥]Biophysics Resource, Structural Biophysics Laboratory, NCI-Frederick, Maryland 21702, and **Molecular Aspects of Drug Design Section, Structural Biophysics Laboratory, NCI-Frederick, Maryland 21702. [††]Passed away on January 9, 2007

ABSTRACT Activation of the signal transducer and activator of transcription 3 (STAT3) is frequently detected in many cancer types. Activated STAT3 may participate in oncogenesis by stimulating cell proliferation and resisting apoptosis, as well as promoting tumor angiogenesis, invasion, and migration. Many STAT3-dependent cellular responses are mediated through interactions with other proteins, and the amino-terminal domain (N-domain) of STAT3 was proposed to be responsible for this. Our NMR studies revealed that synthetic analogs of the STAT4 second α-helix bind to the N-domain and perturb its structure. Structural data available for the STAT4 N-domain was used for the rational design of STAT3 helix 2 analogs with enhanced biological activity. Cell-permeable derivatives of the STAT3 second helix were found to directly and specifically bind to STAT3 but not STAT1 as determined by FRET analysis in cells expressing GFP-STAT3 and GFP-STAT1. Furthermore, they potently induced apoptotic death in breast cancer cells but not normal breast cells or STAT3-deficient fibroblasts. The inhibitors caused significant changes in the mitochondrial potential of cancer cells, leading to cell death. These compounds not only are promising drug candidates but also offer a convenient tool for studying the mechanisms of action of STAT transcription factors and have facilitated our understanding of the crucial role of the N-domain in STAT3 function.

Signal transducer and activator of transcription (STAT) proteins are transcription factors with complex structures and modes of actions that are poorly understood (*1*). All seven STAT proteins in mammals consist of six domains that are called N-domain (ND), coiled-coil, DNA-binding, linker, Src homology 2 (SH2), and transcriptional activation domains. STATs are transiently activated by tyrosine phosphorylation in response to extracellular signals such as cytokines and growth factors (*1, 2*). Phosphorylation triggers STAT dimerization and nuclear accumulation, which facilitates STAT binding to specific DNA-response elements in the promoters of target genes and their transcriptional activation(*1*). Under normal conditions, STAT activation is transient and tightly regulated. In tumor cells, STAT3 is frequently constitutively activated and induces deleteriously prolonged activation of some target genes, such as antiapoptotic genes Bcl-xL, Bcl-2, Mcl-1, and Survivin along with genes driving cell cycle progression, c-Myc and cyclin D1(*3*). STAT3 also suppresses apoptosis by inhibiting the expression of pro-apoptotic genes, such as tumor necrosis factor-related apoptosis-inducing ligand (TRAIL) (*4*) and tyrosine phosphatase tumor suppressor gene SHP-1 (*5*). This implies that suppression of STAT3 activation could facilitate growth arrest and apoptosis in cancer cells (*6*). The deregulation of STAT pathways occurs during development of many types of tumors (*7*). Among STAT family members, aberrant activation of STAT3 is most frequent in almost all blood malignancies and solid tumors, includ-

*Corresponding author, tarasova@ncifcrf.gov.

Received for review September 5, 2007 and accepted November 19, 2007.

Published online December 21, 2007

10.1021/cb700186x CCC: $37.00

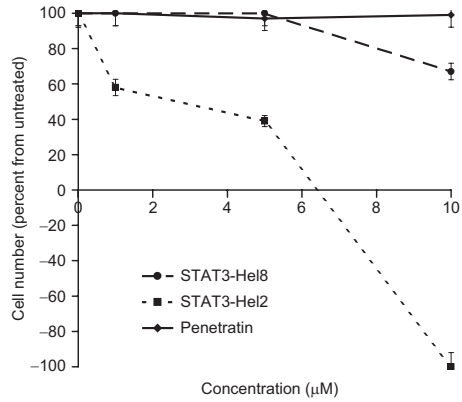

Figure 1. Both helix-2- and helix-8-derived peptides fused to the penetratin sequence inhibited growth of MCF7 breast cancer cells, and the helix 2 derivative also induced cell death. Activity was determined by MTT assay after 48 h exposure to the compounds. STAT3-Hel2 = LDTRY-LEQLHQLYS-penetratin, STAT3-Hel8 = RCLWEESKLLQTA-penetratin, Penetratin = RQIKIWFPNRR-Nle-KWKK-NH_2.

ing lymphoma and leukemia, breast, prostate, lung, head and neck, brain, and colon cancers (*8, 9*). Inhibition of STAT3 signaling leads to the suppression of tumor cell growth and apoptosis (*10*). The tight association of STAT3 activation with transformation and tumor progression has therefore made STAT3 an attractive molecular target for the development of novel cancer therapeutics (*6, 10*). Most currently available inhibitors prevent STAT3 tyrosine phosphorylation. Many of the compounds target abnormally activated upstream kinases, such as Jaks, Src, Egfr, or Erb2 (*10, 11*). Some of the inhibitors directly bind to the SH2 domain of STAT3 and prevent tyrosine phosphorylation, protein dimerization, and transcriptional activity (*6, 12–15*). Although tyrosine phosphorylation represents an important step in the activation of STAT3, it has been shown that even nonphosphorylated STAT3 contributes to carcinogenesis through regulation of gene expression (*16*). It has been proposed that protein–protein interactions between STAT3 and other transcription factors can greatly affect its repertoire of transcriptional activities and contribute to tumorigenesis (*17*). The ND of STAT3 is involved in many protein–protein interactions, which include the interaction of two STAT dimers on neighboring sites to form a more stable tetramer (*18*), the interaction of STAT3 with other transcription factors and cofactors leading to formation of enchanceosomes (*19*), and the interaction with histone-modifier proteins to induce changes in chromatin structure (*20*). These complex interactions provide for maximum STAT3-dependent transcriptional stimulation in normal and cancer cells (*21*). Moreover, the ND has also been implicated in interaction with receptors and in the nuclear translocation of STATs (*22–24*). Nevertheless, the role of ND in the function of STATs is poorly understood. Structural studies of the NDs of STAT1 and STAT4 have suggested that the overall fold of the domain is similar for different STATs. The domains are about 130 residues long and contain eight helices, which comprise most of the NDs. NMR and X-ray crystallography suggested two different modes of domain dimerization for STAT4 (*25, 26*). However, both modes involve the second α-helix of the proteins. We have synthesized a number of targeted libraries of cell-permeable analogs of the STAT3 second helix and have found them to be potent inhibitors of STAT3-dependent cancer cell survival and growth.

RESULTS AND DISCUSSION

The original design of the ND inhibitors was based on the high resolution NMR structure of the STAT4 ND. NMR studies have suggested that the STAT4 ND dimer is formed by two helices: 12-residue-long helix 2 and 20-residue-long helix 8 (*25*). We have synthesized both helices derived from the STAT3 sequence. To enable penetration of the cell membrane, the peptides were fused on the C-terminus to penetratin, the third helix of the homeodomain of the Antennapedia homeoprotein (*27*). The derivative of helix 2 showed much higher growth inhibition and cell-killing activity when tested on MCF-7 breast cancer cells (Figure 1).

Synthetic analogs of STAT4 second and eighth helices were tested for interactions with the whole ND of STAT4 by NMR. Interaction of helix 8 could not be studied in detail because addition of the peptide caused precipitation of the protein, most likely due to significant unfolding. Addition of the helix 2 analog (Ac-EIKFLE-QVDKFY-penetratin) also caused significant conformational changes in the domain, as was evident from the changes in chemical shifts of ^{N}H groups of residues 27, 77, 93, 96, 99, 102, 103, and 114 (Figure 2, panel a). The most pronounced differences in chemical shifts were detected in helix 8, as could be predicted from the structure of the dimer in solution (*25*). The dimer interface demonstrated in the crystal structures of the NDs of STAT4 and STAT1 consists of interacting helices

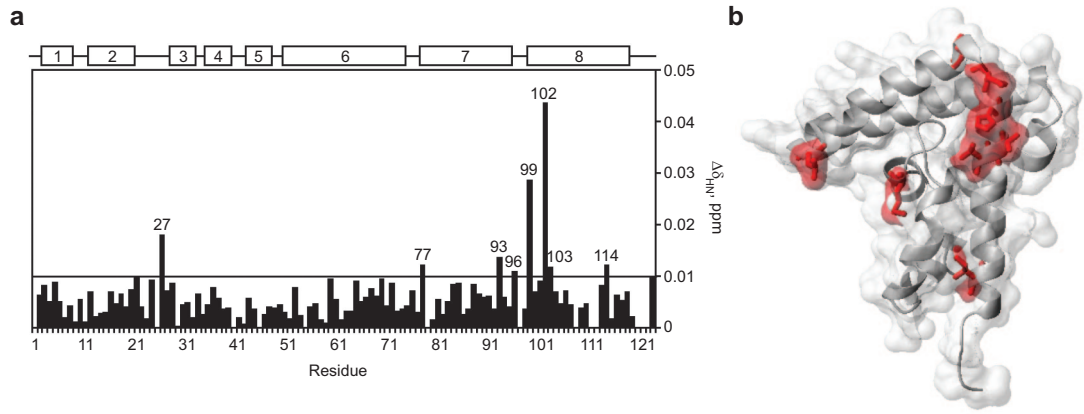

Figure 2. Addition of a helix 2 analog to STAT4 ND caused significant conformational change revealed by NMR. a) Chemical shift changes detected in ^{N}H of the STAT4 ND in the HSQC NMR spectrum upon addition of 1 mol equiv of synthetic peptide corresponding to the helix 2 sequence (Ac-EIKFLEQVDKFY-penetratin). The chemical shift changes were measured for ^{1}H and ^{15}N, combined, and normalized as described in Methods. The boxes above the graph represent the positions of helical regions in the STAT4 ND. The horizontal line shows the average value of chemical shift perturbations plus 1 SD. The residues exhibiting statistically significant chemical shift perturbations are numbered on the graph. b) The most significant chemical shift perturbations were mapped onto the crystal structure of the STAT4 ND (red side chains) generated using MOLMOL software (*29*) and pdb coordinates 1BGF (*30*). The chemical shift perturbations mark a continuous binding site on helix 8 that is colored in red.

2 and 7 (*26, 28*). However, solution-state NMR detects a new set of interactions upon STAT4 dimerization, namely, parallel binding of helix 2 and helix 8 (*25*). Physiological relevance of this novel interface and the crystal dimerization interface awaits further evaluation in the structure of a full-length phosphorylated STAT tetramer assembled on DNA. Nonetheless, helix 2 is predicted to participate in either of these interfaces. Therefore, the helix 2 analog may disrupt dimerization of STAT NDs and/or interfere with the ND interactions with the STAT core. The chemical shift perturbations in residues 96, 99, 102, and 103 delineate a continuous binding site on the surface of STAT4 ND (Figure 2, panel b). Residue 114 is positioned in helix 8 and is responsible for its interactions with helix 2. Residues 93 and 27 are affected because of their proximity to the binding site. The effect of peptide binding on the chemical shift of residue 77 is likely to be secondary because no other significant chemical shift perturbations are detected in the N-terminal part of helix 7. The data suggest that helix 2 analogs do not simply dissociate ND dimers but cause significant conformational changes that are likely to interfere with domain function. The lack of available purified and well-folded STAT3 ND precluded the study of interactions of inhibitors with the intended target by direct methods. Thus, STAT4 data and sequence homology were used to construct corresponding STAT3 helix 2 analogs. Significant cell-killing activity of the compounds encouraged us to study the molecular and cellular mechanisms of peptide activity.

Structure–Activity Relationships in Derivatives of STAT3 Helix 2. To test whether inhibition of ND interactions could suppress STAT3 signaling and growth of cancer cells, a library of synthetic peptide analogs of STAT3 helix 2 was constructed (Table 1). To enable cell membrane penetration, the peptides were fused on the C-terminus to penetratin, which is a 16-amino-acid-long peptide fragment that is internalized by cells in a specific, non-receptor-mediated manner and can be used as an intracellular vehicle for the delivery of oligopeptides and oligonucleotides (*27*). Penetratin efficiently delivered peptide into cells within 30 min of treatment (Supplementary Figure 1).

The ND of STAT3 is involved in the interaction of two STAT dimers on neighboring sites to form a more stable tetramer and enhance transcription from STAT-dependent *cis*-elements. Tostudy the effect of inhibitors on STAT3-dependent transcription, we employed the Mercury JAK-STAT pathway profiling system with the STAT DNA-binding elements GAS (interferon-γ activat-

TABLE 1. Inhibition of cell growth by different variants of the STAT3 second helix[a]

Peptide	Sequence	Cell growth in 5 μM compound, % from control[b]	GAS–luciferase reporter activity in 10 μM compound, % from control
Hel2-Pen	LDTRYLEQLHQLYS_	73 ± 5	56 ± 5
Hel2A-pen	DTRYLEQLHKLYS	44 ± 5	100 ± 9
Hel2B-Pen	LDTRYLEQLHKLYS	82 ± 6	100 ± 9
Hel2C-Pen	DTRYLEQLHKLCyPheS	38 ± 4	NA[c]
Hel2D-Pen	DTKYLEQLHKLYS	42 ± 4	NA
Hel2E-Pen	DTRYLQELHKLYS	46 ± 4	NA
Hel2F-Pen	DTRYLEQLHDabLYS	60 ± 5	NA
Hel2G-Pen	AQWNQLQQLDTRYLEQLHQLYS	80 ± 5	NA
Hel2A-2-Pen	LDTRYLEQLHKLY	65 ± 4	71 ± 6
Hel2A-2a-Pen	DTRYLEQLHKLY	65 ± 5	NA
Ac-Hel2A-2a-Pen	Ac-DTRYLEQLHKLY	45 ± 5	NA
Hel2H-Pen	LDTRYLEQLHDabLY	45 ± 4	43 ± 4
Hel2I-Pen	DTRYLEQLHDabLY	25 ± 4	53 ± 6
Hel2K-Pen	LDTKYLEQLHDabLY	8 ± 2	NA
Hel2A-3-Pen	Ac-DTRYLEQLHALY	93 ± 6	89 ± 9
Hel2A-4-Pen	Ac-DTRYLEQLHELY	91 ± 6	NA
Hel2A-5-Pen	Ac-ATRYLEQLHKLY	85 ± 5	NA

[a]Activity was determined by MTT assay against MCF-7 cells grown in RPMI medium supplemented with 10% fetal bovine serum after 48 h exposure to compounds. Amino acid substitutions in the native sequence are underlined. Penetratin sequence RQIKIWFPNRR-Nle-KWKK-NH_2 was added to the C-termini of all listed peptides. [b]Activity at 5 μM was used as the criterion for activity comparison instead of GI_{50} because very steep activity curves with significant cell killing at 10 μM for many derivatives (Figures 1 and 6) introduced significant errors during GI_{50} determination. [c]Data not available.

ing sequence) introduced as three tandem copies upstream of the TA promoter in a luciferase reporter vector and APRE luciferase reporter plasmids containing four copies of wild-type interleukin-6 (IL-6) response elements of the rat α2-macroglobulin promoter (*31*). MCF-7 cells were transfected with luciferase and renila luciferase (for normalization purposes) reporter vectors. Despite low basal level of tyrosine phosphorylated STAT3 in MCF-7 cells, expression levels of GAS- and APRE-reporters were high. STAT3 helix 2 analogs reduced basal expression of the GAS- and APRE-reporters in MCF-7 cells within 1 h after treatment (Table 1). Luciferase vector with no insertion upstream of the TA promoter and mutant APRE served as negative controls and showed no change in luciferase activity upon treatment. These data suggest that STAT3 helix 2 analogs are able to interfere with STAT3-dependent transcription.

Growth inhibition of MCF-7 cells by STAT3 helix 2 analogs was evaluated by MTT cytotoxicity assay (Table 1). Both MTT and luciferase assays identified STAT3-Hel2A-2 peptide as the most potent. In the solution structure of STAT4 N-domain, Gln20 in helix 2 forms a hydrogen bond with invariant Glu112 of helix 8. We speculated that replacement of a low energy hydrogen bond with a high energy ionic pair by substituting glutamine with a positively charged residue would facilitate the binding of the peptides to the protein. This turned out to be correct, and significant improvements in the potency of peptides were achieved by substituting Gln20 residue with lysine (Hel2A) or diamino-butyric acid, Dab (Hel2H, Hel2I and Hel2K). Improvement of activity was also achieved by substitution of Ser23 with arginine or lysine (Hel2A-2). Interestingly, the peptide corresponding to a fusion of helices 1 and 2 (Hel2G) was less active than helix 2 alone. Based on the improved structure of STAT3-Hel2A-2, we also constructed inhibitory peptides for STAT1(LDSKF-LEQVHKLY-penetratin) and STAT5a (LQGDALRQ-Nle-

```
STAT4:  MSQWNQVQQLEIKFLEQVDQFYDDNFPMEIRHLLAQWIENQDWEA
STAT1:  MSQWYELQQLDSKFLEQVHQLYDDSFPMEIRQYLAQWLEKQDWEH
STAT3:  MAQWNQLQQLDTRYLEQLHQLYSDSFPMELRQFLAPWIESQDWAY
STA5A:  MAGWIQAQQLQGDALRQMQVLYGQHFPIEVRHYLAQWIESQPWDA
STA5B:  MAVWIQAQQLQGEALHQMQALYGQHFPIEVRHYLSQWIESQAWDS
STAT2:  MAQWEMLQNLDSPFQDQLHQLYSHSLLPVDIRQYLAVWIEDQNWQ
                          *  * *
STAT6:  MSLWGLVSKM PPEKVQR  LYVDFPQHLRHLLGDWLESQPWEFLVGS
```

Figure 3. Only two residues in the primary structures of helix 2 (underlined) of different STAT proteins are invariant: Gln17 and Tyr22. Helix 2 of STAT1 and helix 2 of STAT3 are very much alike, showing four conserved substitutions.

TABLE 2. Structure–activity relationships in palmitoylated derivatives of helix2 of STATs[a]

Peptide	Sequence	GI_{50}, μM
ST1-H2-K-Pal	DSKFLEQVHKLYRQIK-ϵ-Pal	>10
ST1-H2-Pal1	Pal-IQRYLKHVQELFKSD (all-D)	0.8 ± 0.1
ST1-H2-Pal2	Pal-IQKYLKHVQELFKSD (all-D)	0.65 ± 0.1
ST5-H2a-K-Pal	LQGDALRQ-Nle-QVLYRQIK-ϵ-Pal	0.45 ± 0.05
ST5-H2–3-K-Pal	QGDALRQ-Nle-QVLYRQIK- ϵ -Pal	0.6 ± 0.1
ST3-H2a-K-Pal	DTKYLEQLHKLYKK- ϵ-Pal	1.05 ± 0.1
ST3-H2a-K-Pal—Cyc1	DTKYcyclo[CEQLK]KLYKK- ϵ-Pal	1.05 ± 0.1
ST3-H2a-K-Pal—Cyc2	DTKcyclo[CLEQK]HKLYKK- ϵ-Pal	1.35 ± 0.3
St3-H2a-2a-Pal1	Pal-IQRYLKHLQELYRTD (all-D)	2.6 ± 0.4
St3-H2a-2a-Pal2	Pal-IQKYLKHLQELYRTD (all-D)	2.1 ± 0.2
St3-H2a-2a-Pal3	Pal-QRYLKHLQELYRTD (all-D)	2.3 ± 0.4
St3-H2a-2a-Pal4	Pal-RYLKHLQELYRTD (all-D)	3.5 ± 0.4
St3-H2a-2a-Pal6	Pal-QKYLKHLQELYRTD (all-D)	4.1 ± 0.3
St3-H2a-2a-Pal7	Pal-KYLKHLQELYRTD (all-D)	1.8 ± 0.2
St3-H2a-2a-Pal8	Pal-IQRYLKHLQQLYRTD (all-D)	3.1 ± 0.4
St3-H2a-2a-Pal9	Pal-IQRYLKHLQQLYRTN (all-D)	1.7 ± 0.2
St3-H2a-2a-Pal10	Pal-YLKHLQELYRTD (all-D)	3.5 ± 0.3
St3-H2a-2a-Pal11	Pal-QRYLKHLQELYRTDL (all-D)	2.7 ± 0.3
St3-H2a-2a-Pal12	Pal-YLKHLQQLYRTN (all-D)	>10
St3-H2a-2-penetratin	LDTRYLEQLHKLY- penetratin	0.58 ± 0.10

[a] GI_{50} (compound concentration causing 50% growth inhibition) values were determined in MCF7 breast cancer cells grown in RPMI medium supplemented with 0.5% FBS after 48 h exposure to compounds.

QVLY-penetratin) (Figure 3), which we are using in parallel to elucidate specific modes of action of different STAT derivatives.

Penetratin is efficient in delivering peptides inside cells; however, *in vivo* application of penetratin conjugates is problematic because of low plasma stability. Lipidation is known to facilitate the crossing of cellular membranes by peptides, though lipopeptides generally are not present in the cytoplasm of the cells but rather exist anchored to the membrane through the lipid. We have substituted penetratin in the derivatives of helix two with ϵ-palmitoyl lysine as a means of introducing palmitoyl residue into the peptide (Table 2). Initially, we preserved three residues of penetratin sequence, RQI, in the lipopeptide derivatives because the presence of a positively charged residue coming from penetratin sequence appeared to be essential for the activity. Further structure–activity relationships (SAR) studies showed that glutamine and isoleucine residues could be removed without a significant decrease in activity. STAT3 and STAT5 derivatives showed significant growth inhibitory activity in breast cancer cells (Table 2), whereas the STAT1 derivative was inactive.

CD spectroscopy studies have demonstrated that palmitoylated peptides have a significant degree of helicity and thus mimic well the original structure of the helix in the protein (Supplementary Figure 2). To stabilize the helical conformation, we have implemented i to i-3 side chain-to-side chain covalent linkages that have been shown to stabilize the helical structures of peptides, thus improving their biological activity (*32–34*). We have used a cyteine-to-lysine coupling strategy. Two versions of the cyclic peptide with a shift in the side chain linkages were synthesized (Table 2). Both had activities comparable with the linear parent peptide, ST3-H2a-K-Pal. We did not get improvement in potency by cyclization probably because the helix formed by the original peptide was already fairly stable, as evident from the comparison of CD spectra (Supplementary Figure 2).

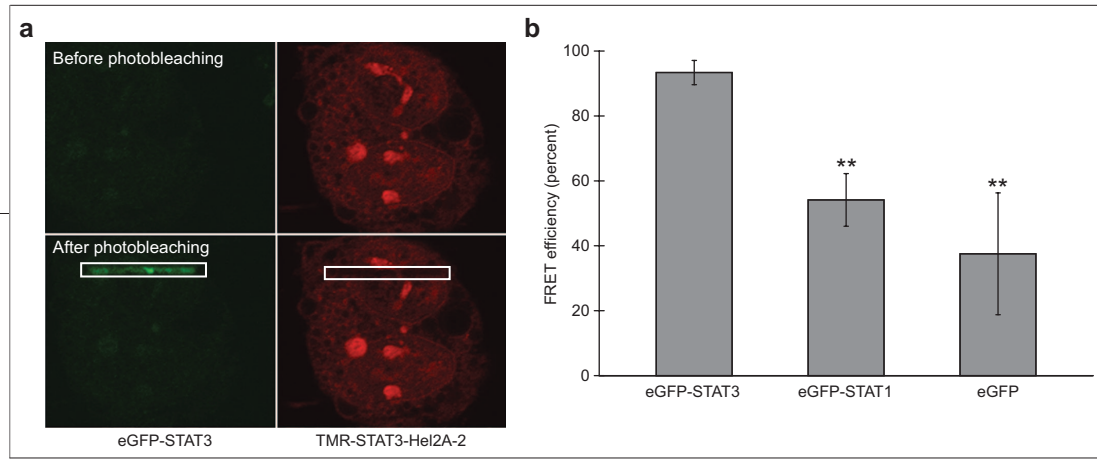

Figure 4. FRET is demonstrated by the acceptor photobleaching method. a) The image of the same HEK293 cell transfected with eGFP-STAT3 and treated with TMR-STAT3-Hel2A-2 before and after photobleaching. A significant increase of the eGFP emission intensity is observed after photobleaching in the region of interest (ROI) contoured by a white line when compared to that before photobleaching. b) The quantitative graphs show the FRET efficiencies of the cells transfected with eGFP-STAT3 (number of cells (n) = 9), eGFP-STAT1 (n = 8), or eGFP (n = 12) treated with TMR-STAT3-Hel2A-2. Columns represent means, bars represent ± SD, ** represents $p < 0.001$ (t-test).

Since regular peptides are known to be unstable in circulation, we attempted to generate all-D analogs of inhibitors by constructing retro-inverso peptides. Inversion of the sequences with simultaneous change in chirality resulted in compounds that were almost as active as their all-L parent peptides in the case of STAT3 and significantly enhanced the cytotoxicity of the STAT1 derivative. We further optimized the structures of the STAT3 derivative by systematic truncation and substitutions of certain critical residues (Table 2). Two N-terminal residues of the original sequence, isoleucine and glutamine, could be eliminated without much change in activity (ST3H2a-2a-Pal3 and ST3H2a-2a-Pal4). The presence of a positively charged residue on the N-terminus of the inverted peptide appeared essential for the activity (ST3-H2a-2a-Pal10 and ST3-H2a-2a-Pal12). Since negative charges can interfere with peptide penetration into the cells, we evaluated the possibility of elimination of aspartic acid and glutamic acid residues in the sequence. C-Terminal aspartic acid could be substituted with asparagine (ST3-H2a-2a-Pal9) even with small gain in activity. Glutamic acid also could be replaced with glutamine but with some loss in potency (ST3-H2a-2a-Pal8). ST3-H2a-2a-Pal7 appeared to be the shortest potent inhibitor, with a length of 13 residues and GI_{50} of 1.8 μM (Table 2).

STAT3 Helix 2 Analogue Interacts with STAT3 in Living Cells. To determine whether STAT3-HEL2A-2 interacts with STAT3 in living cells, we used fluorescence resonance energy transfer (FRET) microscopy, a technique to highlight short-range (less than 10 nm) interactions in live cells (*35*). We have synthesized Hel2 derivative with an additional cysteine residue positioned at the C-terminus of penetratin. Cysteine was used for labeling of the peptide with the maleimide derivative of tetramethyl rhodamine (TMR) to obtain TMR-STAT3-Hel2A-2 peptide. For FRET studies, HEK293 cells, stably transfected with a vector expressing STAT3 tagged with eGFP on its N-terminus (eGFP-STAT3), were treated for 1 h with 5 μM TMR-STAT3-HEL2A-2. Our rationale was that if eGFP-STAT3 and TMR-STAT3-HEL2A-2 interacted and FRET occurred, then photobleaching of the acceptor (TMR) should result in significant increase of donor (eGFP) fluorescence. The acceptor photobleaching and subsequent image analysis were performed as described in Methods. The photobleaching of TMR restored the fluorescence of eGFP, suggesting that TMR-STAT3-HEL2A-2 interacts with e-GFP-STAT3 (Figure 4, panel a). FRET efficiency (E_F) was very high (93.38 ± 3.34%), suggesting tight binding (Figure 4, panel b).

To evaluate selectivity of the peptide toward STAT3 in living cells, we measured FRET in cells expressing eGFP-STAT1 or eGFP treated with TMR-STAT3-H2A-2. Figure 4, panel b demonstrates that binding to eGFP-STAT1 and eGFP was significantly less efficient compared to STAT3. There was no significant difference in peptide binding to eGFP-STAT1 and eGFP ($p = 0.13$). As a negative control, we performed acceptor photobleaching for cells transfected with eGFP-STAT3, eGFP-STAT1, and eGFP expressing constructs but not treated with TMR-STAT3-Hel2A-2. In this situation, FRET should not be possible because the acceptor fluorophore TMR is absent. Indeed, FRET efficiency was very low, −2.67 ± 4.27% (n = 5), 0.97 ± 6.06% (n = 5), and −0.60 ± 2.16% (n = 5) for eGFP-STAT3, eGFP-STAT1, and eGFP, respectively, and in all cases significantly different ($p < 0.001$) from cells treated with TMR-STAT3-Hel2A-2. These results demonstrate that there is no artifactual photoactivation of GFP during acceptor photobleaching and indicate some nonspecific binding of TMR-STAT3-H2A-2 to GFP and eGFP-STAT1. Binding to STAT1 is not surprising because STAT3 is known to form heterodimerswith STAT1,

and thus the observed interaction of the peptide may be indirect. However, because of the very high structural homology between STAT3 and STAT1 NDs, direct interaction of the inhibitors with STAT1 can not be excluded. Nevertheless, our data demonstrate that STAT3-H2A-2 preferentially binds to STAT3 in living cells and might be a useful tool in elucidating novel functions of the STAT3 N-domain and validating it as a drug target.

STAT3-Hel2A-2 Affects STAT3 but Not STAT1 Cytokine-Induced Activation. To further evaluate specificity of STAT3-Hel2A-2 toward STAT3, we assessed effects of the inhibitor on cytokine-stimulated STAT3 and STAT1 signaling pathways in breast cancer cells. We treated MCF-7 and MDA-MB-231 cells with leukemia inhibitory factor (LIF) to activate STAT3 and with interferon γ (IFNγ) to activate STAT1 signaling (Figure 5, panel a). We found that LIF induced selective STAT3 tyrosine phosphorylation, and IFNγ induced selective STAT1 tyrosine phosphorylation only in MCF-7 cells. In MDA-MB-231 cells, both cytokines induced both STAT3 and STAT1 tyrosine phosphorylation. We also found that pretreatment with STAT3-Hel2A-2 or STAT1-Hel2A-2 for 1 h did not affect tyrosine phosphorylation of STAT3 and STAT1. The inhibitors did not change expression levels of STAT3 and STAT1 proteins as well. These data support recently published report that the STAT3 N-domain is not required for tyrosine phosphorylation (*36*). To evaluate effects of inhibitors on cytokine-activated transcription, we employed luciferase reporter vectors APRE (*31*) and ISRE (*37*). APRE was activated in MCF-7 cells by LIF (Figure 5, panel b), and both STAT3-Hel2A-2 and STAT1-Hel2A-2 inhibited basal and stimulated expression. ISRE reporter, containing three tandem copies of STAT1-STAT2 dimers DNA binding sites (*37, 37*), was activated in MCF-7 cells by IFNγ, and only STAT1-Hel2A-2 inhibitor prevented cytokine-stimulated reporter activation (Figure 5, panel c). Taken together, our data demonstrate that STAT3-Hel2A-2 inhibitor specifically inhibits STAT3- but not STAT1-dependent transcription without affecting the levels of STAT3 protein expression or STAT3 tyrosine phosphorylation.

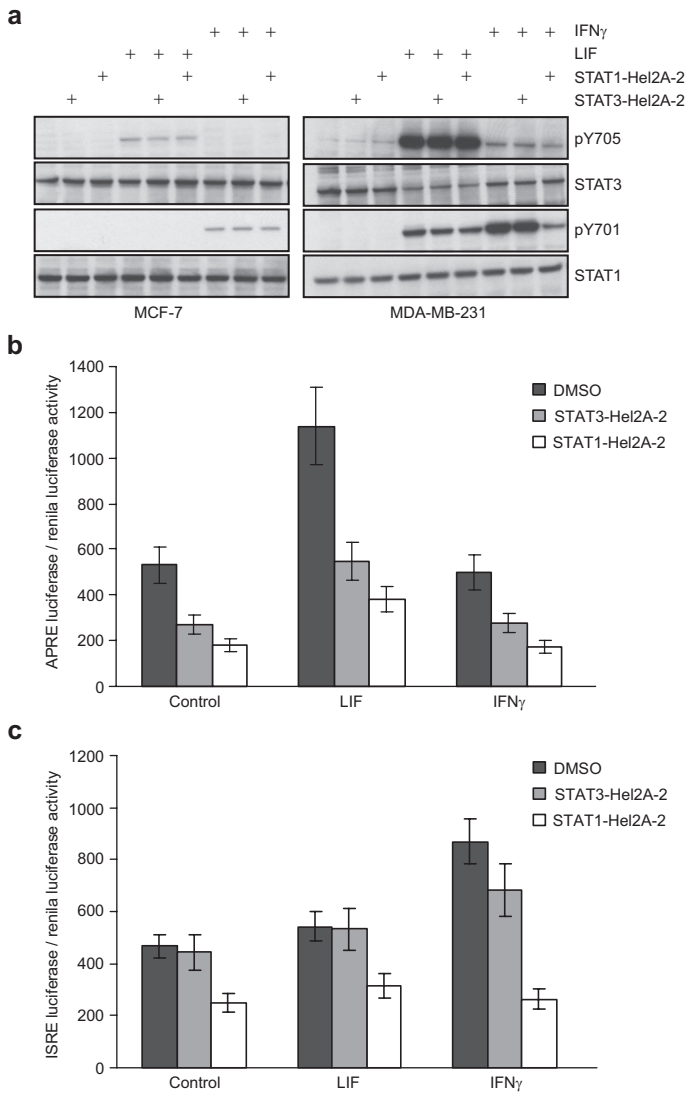

Figure 5. Effect of STAT inhibitors on STAT3 and STAT1 cytokine-induced activation in MCF-7 cells. a) STAT3-Hel2A-2 does not prevent LIF- or IFNγ-induced tyrosine phosphorylation of STAT3 and STAT1. b) STAT3-Hel2A-2 inhibits basal level and LIF-stimulated activation of APRE luciferase reporter, but c) does not affect basal and IFNγ-activated expression of ISRE luciferase reporter.

STAT3-Hel2A Inhibits Survival of Breast Cancer Cells. To evaluate the effect of STAT3-Hel2A on cell proliferation of human breast cancer cell lines, we treated MDA-MB-231, T47D, and MDA-MB-435 cells with escalating doses of STAT3-Hel2A. Cell proliferation and cell death were estimated by the MTT assay, as described in Methods. Figure 6, panel a demonstrates that STAT3 induced death of MDA-MB-231 and MDA-MB-435 breast cancer cells and inhibited proliferation of T47D cells in a dose-dependent manner. Lower sensitivity of MCF-7 and T47D cells compared to MDA-MB-231 and MDA-MB-435 cells correlates well with the level of basal STAT3 activation. MCF-7 and T47D cells have low levels of activated STAT3, whereas MDA-MB-231 and MDA-

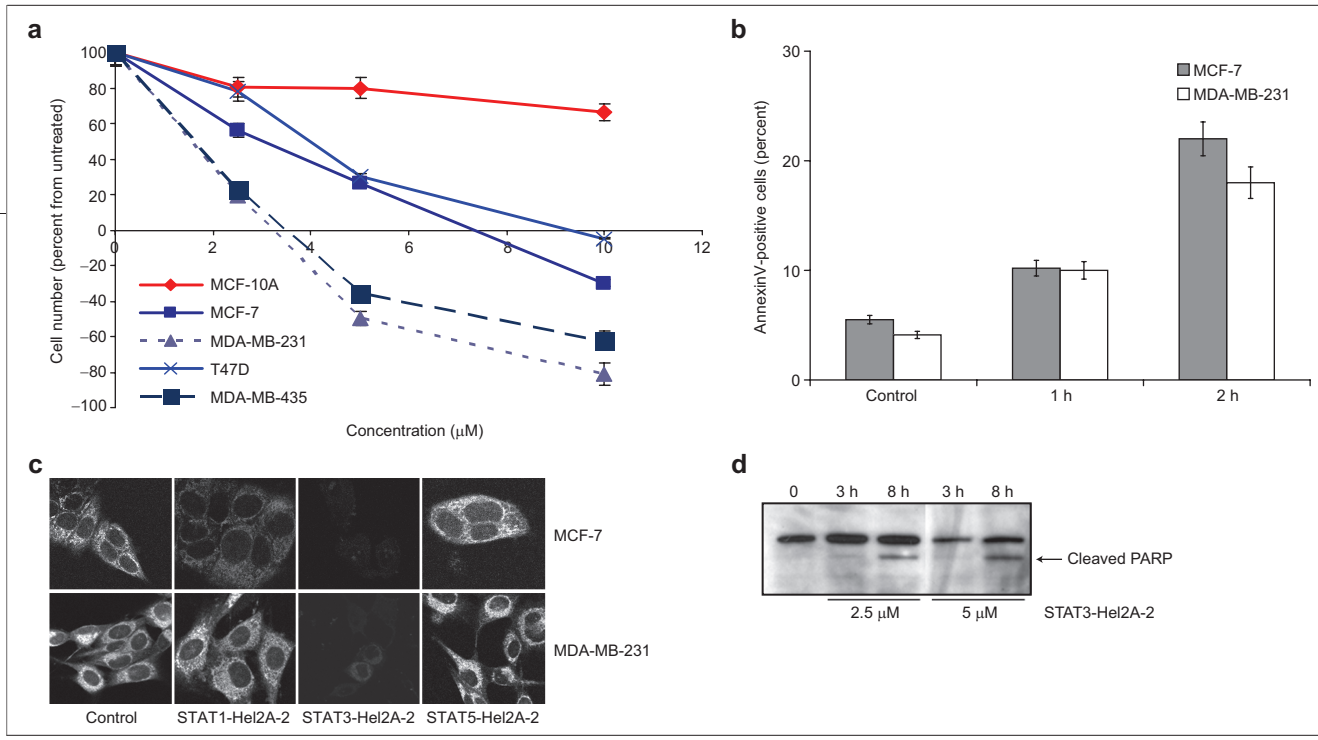

Figure 6. STAT3-Hel2A-2 induces death of breast cancer cells. a) Toxicity of STAT3-Hel2A-2 on normal breast epithelial (MCF-10A) cells and breast cancer cells after 2 days of exposure. b) Annexin V binding is increased in MCF-7 and MDA-MB-231 cells after treatment with STAT3-Hel2A-2. c) STAT3-Hel2A-2 caused a decrease in mitochondrial potential in MCF-7 and MDA-MD-231 cells, detected by staining with MitoTracker Red CMXRos and confocal laser scanning microscopy. d) STAT3-Hel2A-2 induced PARP cleavagedetected by Western blot analysis of treated MDA-MB-231 cells using anti-PARP antibodies.

MB-435 have elevated levels of tyrosine 705-phosphorylated STAT3 (*38*, *39*). The fact that survival of MCF-7 and T47D cells is also affected by inhibition of STAT3 is in agreement with the previously published observation that even unphosphorylated STAT3 has an important role in oncogenesis and might be a promising target for tumor therapy (*16*). In addition, growth and viability of normal mammary epithelial cells MCF-10A were not altered significantly (Figure 6, panel a). Furthermore, survival of normal mouse embryonic fibroblasts (MEFs) and STAT3-deficient MEFs was not affected by treatment with STAT3-Hel2A-2 (data not shown). Our data along with published reports (*40*) show that survival of many tumor-derived cell lines depends on the activity of STAT3, whereas normal cells are perfectly viable without STAT3. This observation potentially provides a basis for an enhanced therapeutic ratio based on differential inhibitor effects

STAT3-Hel2A-2 Preferentially Induces Apoptosis of Breast Cancer Cells. To determine whether the STAT3-Hel2A-2-induced loss of tumor cell viability was due to apoptosis, the human breast carcinoma cell lines MDA-MB-231 and MCF-7 were treated with STAT3-Hel2A-2 or 0.05% DMSO as a control for 2 h and analyzed by annexin V binding and flow cytometry. At 5 μM, STAT3-Hel2A-2 induced a significant increase in Annexin V binding in both cell lines in 2 h (Figure 6, panel b). Morphological changes in the cells could be observed within minutes after addition of the peptides conjugated to penetratin (Supplementary Figure 1). The cellular mechanisms responsible for those rapid changes are currently under investigation. Dose–response curves showed sharp increase in activity over a small range of concentration (Figure 6, panel a). Lack of a gradual increase in activity may be due to a high concentration of the target protein. It was shown that STAT3 is expressed in human T-cells (Jurkat cells) at levels that are about 100-fold higher than STAT1 or HIF-1α (*41*). The reported levels of 100–200 pg/100 cells are equivalent to intracellular concentrations of at least 5–10 μM. Thus, the observed concentration-dependent toxicity curves may be reflecting the titration of a protein that is present in significant quantities.

To further confirm an apoptotic mechanism of cell death, we used *in situ* measurement of mitochondrial membrane potential ($\Delta\Psi$) using a MitoTracker Red CMXRos (Invitrogen), a red-fluorescent dye that stains mitochondria in live cells. Its accumulation is dependent upon membrane potential (*42*). Our data show that treatment with STAT3-Hel2A-2 causes more than 50% of MDA-MB-231 and MCF-7 cells to decrease mitochondrial membrane potential, which leads to apoptosis (Figure 6, panel b). Additionally, we analyzed the degree of poly(ADP-ribose) polymerase (PARP) cleavage, a marker of caspase-dependent apoptosis. MCF-7 cells are caspase-3 deficient, and for this reason we could not evaluate PARP cleavage in this cell line. In MDA-MB-231 cells, significant PARP cleavage was detected after

8 h of treatment with STAT3-Hel2A-2 (Figure 6, panel d). Interestingly, though STAT1 and STAT5b inhibitors decreased survival of breast cancer cells with almost the same efficiency as STAT3 derivatives, they had little, if any, effect on PARP cleavage and mitochondrial membrane potential. The observed effects of STAT3 inhibition on mitochondrial function are in agreement with described STAT3 localization in mitochondria and its essential role in the function of these organelles (*43*). Toxicity of STAT1 and STAT5b helix 2 analogs is in agreement with previously observed induction of apoptosis in breast cancer cells by down-regulation of STAT1 and STAT5b (*44*). However, the selectivity of corresponding compounds has not been characterized yet, and thus any conclusions on the roles of STAT1 and STAT5b NDs would be premature. STAT4 helix 2 derivatives were nontoxic for breast cancer cells.

Taken together, our data demonstrate that STAT3-Hel2A is effective in inducing apoptosis in breast cancer cells, probably through changes in the mitochondrial membrane potential that result in activation of caspases.

Although FRET studies have demonstrated direct and selective interactions of helix-2 derivatives with corresponding STAT proteins, the interactions with other STAT partners cannot be excluded. The STAT NDs are known to be involved in many protein–protein interactions, and thus the peptides can mimic STAT itself in association with corresponding protein partners. Our preliminary data suggest that the inhibitors prevent association of STAT3 with histone deacetylase HDAC1 and DNA methyltransferase DNMT1. The molecular mechanisms of inhibitor-induced cell toxicity are currently under investigation. Past targeting efforts have focused on disrupting the STAT3 SH2 domain because of its role in dimerization, whereas the ND was related to secondary regulatory functions. Our data suggest that the ND has a much broader and more significant role in the function of STAT3. The remarkable and selective toxicity of helix 2 derivatives suggests that STAT3 N-domain is indeed a promising drug target and optimized inhibitors have a potential of becoming effective antitumor agents.

METHODS

NMR Titration. ^{15}N HSQC spectra were acquired for the ^{15}N STAT4 N-domain and the complex of ^{15}N STAT4 N-domain and helix 2 peptide in 50 mM sodium acetate at pH 5.3, 50 mM NaCl, 1 mM DTT, and 10% $^{2}H_2O$ at 1:0, 1:0.2, and 1:1 molar ratios. The concentration of the ^{15}N STAT4 N-domain was 0.8 mM. The spectra were acquired on a 600 MHz Varian spectrometer at 25 °C. The data were processed and analyzed using NMRPipe software (*45*). The ^{N}H and ^{15}N chemical shift perturbations were normalized and combined as a geometric average of the total chemical shift perturbation in ppm:

$$\Delta\delta_{HN} = \sqrt{\frac{(\Delta\delta^{N}H)^2 + (\Delta\delta N)^2/25}{2}}$$

Cell Lines and Expression Vectors. MCF-7, MDA-MB-231, MDA-MB-435, and T47cell lines were cultivated in RPMI medium with 10% FBS, and MCF-10A and HEK293 cells were cultivated in DMEM-F12 with 10% FBS. All cell lines were from the American Type Culture Collection (ATCC). HEK293 cells were stably transfected with vectors expressing eGFP, eGFP-STAT3, or eGFP-STAT1. The STAT3 and STAT1 full-size coding regions were amplified using total cDNA from HEK293 cells and cloned into an eGFP-C1 vector from Clontech, as described previously (*46*). GAS, ISRE, and TA luciferase reporter vectors were from Clontech. APRE and mutant APRE reporter containing four copies of wild-type or mutant interleukin-6 (IL-6) response elements of the rat α2-macroglobulin promoter, respectively, were generous gifts from Dr. T. Takeda (Osaka University Medical School, Osaka, Japan).

Confocal Imaging and Acceptor-Photobleaching Experiment. HEK293 cells stably transfected with e-GFP-STAT3, eGFP-STAT1, or eGFP expression vectors were seeded on poly-L-lysine-coated dishes with cover glass bottoms (Mattek) in DMEM medium without phenol red supplemented with 10% FBS. The following day, cells were treated with 5 μM TMR-ST3-Hel2A-2 for 1 h, and then FRET was measured by the acceptor photobleaching method on live cells. A Zeiss LSM510 confocal microscope (Carl Zeiss, Inc.) was used. Cells were examined with a 63X, 1.4 NA Zeiss oil immersion objective and 2X zoom. Emission filters were 505–550 nm for 488nm excitation and 575–615 nm for 561 nm excitation. To minimize the effect of photobleaching due to imaging, images were collected at 1% of the laser intensity. To ensure that bleaching due to imaging was minimal, we monitored the level of bleaching in each experiment by collecting two eGFP/TMR image pairs before bleaching and two after bleaching. We bleached cells in the TMR channel by scanning a region of interest (ROI) 50 times using the 561 laser line at 100% intensity. Since TMR photobleaching was less than 80%, we calculated the FRET energy transfer efficiency (E_F) using the formula $E_{F(\%)} = E'_{F(\%)}/(1 - \alpha + \alpha E'_{F(\%)})$, where $E'_{F(\%)} = (1 - D_0/D_1) \times 100\%$ is the energy transfer efficiency when the acceptor is 100% photobleached, D_0 and D_1 are eGFP (donor) fluorescent intensity before and after TMR photobleaching, respectively, in the ROI. $\alpha = A_1/A_0$ is the remaining fraction of acceptor that is not photobleached, where A_0 and A_1 are TMR (acceptor) fluorescence intensity before and after photobleaching, respectively, in the ROI. Since fluorescence of eGFP before photobleaching was relatively low (as a consequence of FRET), we always performed background subtraction to correct fluorescence intensities of donor and acceptor.

Acknowledgment: This project was funded in part with federal funds from the National Cancer Institute (NCI), National Institutes of Health under contract N01-CO-12400. This research was supported in part by the Intramural Research Program of the NIH, National Cancer Institute, Center for Cancer Research.

Supporting Information Available: This material is free of charge *via* the Internet.

REFERENCES

1. Levy, D. E., and Darnell, J. E., Jr. (2002) Stats: transcriptional control and biological impact, *Nat. Rev. Mol. Cell Biol. 3*, 651–662.
2. Inghirami, G., Chiarle, R., Simmons, W. J., Piva, R., Schlessinger, K., and Levy, D. E. (2005) New and old functions of STAT3: a pivotal target for individualized treatment of cancer, *Cell Cycle 4*, 1131–1133.
3. Bromberg, J. F., Wrzeszczynska, M. H., Devgan, G., Zhao, Y., Pestell, R. G., Albanese, C., and Darnell, J. E., Jr. (1999) Stat3 as an oncogene, *Cell 98*, 295–303.
4. Niu, G., Shain, K. H., Huang, M., Ravi, R., Bedi, A., Dalton, W. S., Jove, R., and Yu, H. (2001) Overexpression of a dominant-negative signal transducer and activator of transcription 3 variant in tumor cells leads to production of soluble factors that induce apoptosis and cell cycle arrest, *Cancer Res. 61*, 3276–3280.
5. Zhang, Q., Wang, H. Y., Marzec, M., Raghunath, P. N., Nagasawa, T., and Wasik, M. A. (2005) STAT3- and DNA methyltransferase 1-mediated epigenetic silencing of SHP-1 tyrosine phosphatase tumor suppressor gene in malignant T lymphocytes, *Proc. Natl. Acad. Sci. U.S.A. 102*, 6948–6953.
6. Aggarwal, B. B., Sethi, G., Ahn, K. S., Sandur, S. K., Pandey, M. K., Kunnumakkara, A. B., Sung, B., and Ichikawa, H. (2006) Targeting signal-transducer-and-activator-of-transcription-3 for prevention and therapy of cancer: modern target but ancient solution, *Ann. N.Y. Acad. Sci. 1091*, 151–169.
7. Haura, E. B., Turkson, J., and Jove, R. (2005) Mechanisms of disease: Insights into the emerging role of signal transducers and activators of transcription in cancer, *Nat. Clin. Pract. Oncol. 2*, 315–324.
8. Jing, N., and Tweardy, D. J. (2005) Targeting Stat3 in cancer therapy, *Anticancer Drugs 16*, 601–607.
9. Chiarle, R., Simmons, W. J., Cai, H., Dhall, G., Zamo, A., Raz, R., Karras, J. G., Levy, D. E., and Inghirami, G. (2005) Stat3 is required for ALK-mediated lymphomagenesis and provides a possible therapeutic target, *Nat. Med. 11*, 623–629.
10. Deng, J., Grande, F., and Neamati, N. (2007) Small molecule inhibitors of Stat3 signaling pathway, *Curr. Cancer Drug Targets 7*, 91–107.
11. Iwamaru, A., Szymanski, S., Iwado, E., Aoki, H., Yokoyama, T., Fokt, I., Hess, K., Conrad, C., Madden, T., Sawaya, R., Kondo, S., Priebe, W., and Kondo, Y. (2007) A novel inhibitor of the STAT3 pathway induces apoptosis in malignant glioma cells both in vitro and in vivo, *Oncogene 26*, 2435–2444.
12. Schust, J., Sperl, B., Hollis, A., Mayer, T. U., and Berg, T. (2006) Stattic: a small-molecule inhibitor of STAT3 activation and dimerization, *Chem. Biol. 13*, 1235–1242.
13. Siddiquee, K., Zhang, S., Guida, W. C., Blaskovich, M. A., Greedy, B., Lawrence, H. R., Yip, M. L., Jove, R., McLaughlin, M. M., Lawrence, N. J., Sebti, S. M., and Turkson, J. (2007) Selective chemical probe inhibitor of Stat3, identified through structure-based virtual screening, induces antitumor activity, *Proc. Natl. Acad. Sci. U.S.A. 104*, 7391–7396.
14. Ren, Z., Cabell, L. A., Schaefer, T. S., and McMurray, J. S. (2003) Identification of a high-affinity phosphopeptide inhibitor of Stat3, *Bioorg. Med. Chem. Lett. 13*, 633–636.
15. Coleman, D. R., Ren, Z., Mandal, P. K., Cameron, A. G., Dyer, G. A., Muranjan, S., Campbell, M., Chen, X., and McMurray, J. S. (2005) Investigation of the binding determinants of phosphopeptides targeted to the SRC homology 2 domain of the signal transducer and activator of transcription 3. Development of a high-affinity peptide inhibitor, *J. Med. Chem. 48*, 6661–6670.
16. Yang, J., Chatterjee-Kishore, M., Staugaitis, S. M., Nguyen, H., Schlessinger, K., Levy, D. E., and Stark, G. R. (2005) Novel roles of unphosphorylated STAT3 in oncogenesis and transcriptional regulation, *Cancer Res. 65*, 939–947.
17. Shuai, K. (2000) Modulation of STAT signaling by STAT-interacting proteins, *Oncogene 19*, 2638–2644.
18. Xu, X., Sun, Y. L., and Hoey, T. (1996) Cooperative DNA binding and sequence-selective recognition conferred by the STAT amino-terminal domain, *Science 273*, 794–797.
19. Zhang, X., and Darnell, J. E., Jr. (2001) Functional importance of Stat3 tetramerization in activation of the alpha 2-macroglobulin gene, *J. Biol. Chem. 276*, 33576–33581.
20. Zhang, Y., Sif, S., and Dewille, J. (2007) The mouse C/EBPdelta gene promoter is regulated by STAT3 and Sp1 transcriptional activators, chromatin remodeling and c-Myc repression, *J. Cell Biochem*.
21. Shuai, K. (2000) Modulation of STAT signaling by STAT-interacting proteins, *Oncogene 19*, 2638–2644.
22. Tyler, D. R., Persky, M. E., Matthews, L. A., Chan, S., and Farrar, J. D. (2007) Pre-assembly of STAT4 with the human IFN-alpha/beta receptor-2 subunit is mediated by the STAT4 N-domain, *Mol. Immunol. 44*, 1864–1872.
23. Ota, N., Brett, T. J., Murphy, T. L., Fremont, D. H., and Murphy, K. M. (2004) N-domain-dependent nonphosphorylated STAT4 dimers required for cytokine-driven activation, *Nat. Immunol. 5*, 208–215.
24. Zhang, T., Kee, W. H., Seow, K. T., Fung, W., and Cao, X. (2000) The coiled-coil domain of Stat3 is essential for its SH2 domain-mediated receptor binding and subsequent activation induced by epidermal growth factor and interleukin-6, *Mol. Cell. Biol. 20*, 7132–7139.
25. Byrd, R., Gaponenko, V., Sarma, S. P., Tarasova, N. I., Li, J. J., and Altieri, A. S. (2002) New insights into dimerization of STAT proteins: A vehicle to modulate signaling for therapeutic purposes? *Proc. Am. Assoc. Cancer Res. 43*, 139.
26. Chen, X., Vinkemeier, U., Zhao, Y., Jeruzalmi, D., Darnell, J. E., Jr., and Kuriyan, J. (1998) Crystal structure of a tyrosine phosphorylated STAT-1 dimer bound to DNA, *Cell 93*, 827–839.
27. Mae, M., and Langel, U. (2006) Cell-penetrating peptides as vectors for peptide, protein and oligonucleotide delivery, *Curr. Opin. Pharmacol. 6*, 509–514.
28. Zhong, M., Henriksen, M. A., Takeuchi, K., Schaefer, O., Liu, B., ten, H. J., Ren, Z., Mao, X., Chen, X., Shuai, K., and Darnell, J. E., Jr (2005) Implications of an antiparallel dimeric structure of nonphosphorylated STAT1 for the activation-inactivation cycle, *Proc. Natl. Acad. Sci. U.S.A. 102*, 3966–3971.
29. Koradi, R., Billeter, M., and Wuthrich, K. (1996) MOLMOL: a program for display and analysis of macromolecular structures, *J. Mol. Graphics 14*, 51–32.
30. Vinkemeier, U., Moarefi, I., Darnell, J. E., Jr., and Kuriyan, J. (1998) Structure of the amino-terminal protein interaction domain of STAT-4, *Science 279*, 1048–1052.
31. Takeda, T., Kurachi, H., Yamamoto, T., Nishio, Y., Nakatsuji, Y., Morishige, K., Miyake, A., and Murata, Y. (1998) Crosstalk between the interleukin-6 (IL-6)-JAK-STAT and the glucocorticoid-nuclear receptor pathway: synergistic activation of IL-6 response element by IL-6 and glucocorticoid, *J. Endocrinol. 159*, 323–330.
32. Leduc, A. M., Trent, J. O., Wittliff, J. L., Bramlett, K. S., Briggs, S. L., Chirgadze, N. Y., Wang, Y., Burris, T. P., and Spatola, A. F. (2003) Helix-stabilized cyclic peptides as selective inhibitors of steroid receptor-coactivator interactions, *Proc. Natl. Acad. Sci. U.S.A. 100*, 11273–11278.
33. Bernal, F., Tyler, A. F., Korsmeyer, S. J., Walensky, L. D., and Verdine, G. L. (2007) Reactivation of the p53 tumor suppressor pathway by a stapled p53 peptide, *J. Am. Chem. Soc. 129*, 2456–2457.
34. Walensky, L. D., Kung, A. L., Escher, I., Malia, T. J., Barbuto, S., Wright, R. D., Wagner, G., Verdine, G. L., and Korsmeyer, S. J. (2004) Activation of apoptosis in vivo by a hydrocarbon-stapled BH3 helix, *Science 305*, 1466–1470.

35. Kenworthy, A. K. (2001) Imaging protein-protein interactions using fluorescence resonance energy transfer microscopy, *Methods 24*, 289–296.
36. Zhang, L., Badgwell, D. B., Bevers, J. J., III, Schlessinger, K., Murray, P. J., Levy, D. E., and Watowich, S. S. (2006) IL-6 signaling via the STAT3/SOCS3 pathway: functional analysis of the conserved STAT3 N-domain, *Mol. Cell. Biochem. 288*, 179–189.
37. Ivanova, A. V., Ivanov, S. V., Zhang, X., Ivanov, V. N., Timofeeva, O. A., and Lerman, M. I. (2004) STRA13 interacts with STAT3 and modulates transcription of STAT3-dependent targets, *J. Mol. Biol. 340*, 641–653.
38. Sun, J., Blaskovich, M. A., Jove, R., Livingston, S. K., Coppola, D., and Sebti, S. M. (2005) Cucurbitacin Q: a selective STAT3 activation inhibitor with potent antitumor activity, *Oncogene 24*, 3236–3245.
39. Sasser, A. K., Sullivan, N. J., Studebaker, A. W., Hendey, L. F., Axel, A. E., and Hall, B. M. (2007) Interleukin-6 is a potent growth factor for ER-{alpha}-positive human breast cancer, *FASEB J. 21*, 3763–3770.
40. Schlessinger, K., and Levy, D. E. (2005) Malignant transformation but not normal cell growth depends on signal transducer and activator of transcription 3, *Cancer Res. 65*, 5828–5834.
41. Phillips, T. M., and Smith, P. (2003) Analysis of intracellular regulatory proteins by immunoaffinity capillary electrophoresis coupled with laser-induced fluorescence detection, *Biomed. Chromatogr. 17*, 182–187.
42. Gilmore, K., and Wilson, M. (1999) The use of chloromethyl-X-rosamine (Mitotracker red) to measure loss of mitochondrial membrane potential in apoptotic cells is incompatible with cell fixation, *Cytometry 36*, 355–358.
43. Potla, R., Koeck, T., Wegrzyn, J., Cherukuri, S., Shimoda, K., Baker, D. P., Wolfman, J., Planchon, S. M., Esposito, C., Hoit, B., Dulak, J., Wolfman, A., Stuehr, D., and Larner, A. C. (2006) Tyk2 tyrosine kinase expression is required for the maintenance of mitochondrial respiration in primary pro-B lymphocytes, *Mol. Cell. Biol. 26*, 8562–8571.
44. Yamashita, H., Iwase, H., Toyama, T., and Fujii, Y. (2003) Naturally occurring dominant-negative Stat5 suppresses transcriptional activity of estrogen receptors and induces apoptosis in T47D breast cancer cells, *Oncogene 22*, 1638–1652.
45. Delaglio, F., Grzesiek, S., Vuister, G. W., Zhu, G., Pfeifer, J., and Bax, A. (1995) NMRPipe: a multidimensional spectral processing system based on UNIX pipes, *J. Biomol. NMR 6*, 277–293.
46. Timofeeva, O. A., Plisov, S., Evseev, A. A., Peng, S., Jose-Kampfner, M., Lovvorn, H. N., Dome, J. S., and Perantoni, A. O. (2006) Serine-phosphorylated STAT1 is a prosurvival factor in Wilms' tumor pathogenesis, *Oncogene 25*, 7555–7564.